

Low-noise quantum frequency conversion in a monolithic cavity with bulk periodically poled potassium titanyl phosphate

Felix Mann,^{1,*} Helen M. Chrzanowski,¹ Felipe Gewers,² Marlon Placke,¹ and Sven Ramelow^{1,3}

¹ Institut für Physik, Humboldt-Universität zu Berlin, Newtonstraße 15, 12489 Berlin, Germany

² Instituto de Física, Universidade de São Paulo, Rua do Matão 1371, São Paulo, 05315-970, Brazil

³ IRIS Adlershof, Humboldt-Universität zu Berlin, Zum Großen Windkanal 2, 12489 Berlin, Germany

(Received 20 June 2023; revised 24 June 2023; accepted 16 October 2023; published 3 November 2023)

Interfacing the different building blocks of a future large-scale quantum network will require efficient and noiseless frequency conversion of quantum light. Nitrogen-vacancy centers in diamond are a leading candidate to form the nodes of such a network. However, the performance of a suitable converter remains a bottleneck, with existing demonstrations severely limited by parasitic noise arising at the target telecommunication wavelength. Here we demonstrate a platform for efficient low-noise quantum frequency conversion based on a monolithic bulk periodically poled potassium titanyl phosphate cavity and show its suitability for the conversion of 637-nm single photons from nitrogen-vacancy centers in diamond to telecommunication wavelengths. By resonantly enhancing the power of an off-the-shelf pump laser, we achieve an internal conversion efficiency of $(72.3 \pm 0.4)\%$ while generating noise of only (110 ± 4) kHz/nm at the target wavelength without the need for any active stabilization. This constitutes a fivefold reduction in noise over existing state-of-the-art single-step converters at these wavelengths. We verify the almost-ideal preservation of nonclassical correlations by converting photons from a spontaneous-parametric-down-conversion source and moreover show the preservation of time-energy entanglement via Franson interferometry.

DOI: 10.1103/PhysRevApplied.20.054010

I. INTRODUCTION

Quantum frequency conversion (QFC), the coherent interchange of quantum states between light beams of different frequencies [1], will be indispensable for interfacing the different building blocks of future heterogeneous quantum networks [2,3]. Several platforms are currently being extensively investigated for the implementation of such networks: trapped ions [4], atoms [5], semiconductor quantum dots [6], and color centers in diamond [7]. Here specifically, nitrogen-vacancy (N-V) centers in diamond are a promising platform [8,9]. This is due to the long coherence time of the electronic spin associated with this defect center [10], the possibility to couple this electronic spin to nuclear spin [11–13], and an optical interface at 637 nm [14]. Thus, N-V centers in diamond have the potential of being used to process, store, and transmit quantum information [15].

Without the conversion of the N-V center’s 637-nm single photons to the telecommunication band, they suffer from strong transmission losses in optical fiber, severely limiting the suitability of N-V centers for large-scale quantum networks [16]. As a potential solution, efficient QFC

of single photons has been demonstrated with use of sum-frequency generation (SFG) or difference-frequency generation (DFG) driven by a strong pump laser. QFC by SFG or DFG is usually realized in periodically poled $\chi^{(2)}$ -nonlinear crystals, with the conversion efficiency η_c as a function of pump power P_p given by [17]

$$\eta_c = \sin^2 \left(\frac{\pi}{2} \sqrt{\frac{P_p}{P_{\max}}} \right),$$

$$P_{\max} = \frac{c \epsilon_0 n_t n_r \lambda_t \lambda_r \lambda_p}{128 d_{\text{eff}}^2 L h_m(\xi_p, \xi_r)},$$
(1)

where λ_x is the vacuum wavelength, where subscript t denotes the target wavelength (or telecommunication wavelength), subscript r denotes the input, “red” wavelength, and subscript p denotes the pump wavelength, and n_x denotes the corresponding refractive indices. Further, d_{eff} is the nonlinear coefficient, L is the length of the nonlinear crystal, and h_m is the reduction factor for focused Gaussian beams, which is a function of the focusing parameters ξ_x of the participating beams [18,19].

The central challenge for all implementations of frequency converters—for which periodically poled lithium niobate (PPLN) waveguides have historically been the

* felixmann@physik.hu-berlin.de

favored architecture—is noise arising at the target conversion wavelength [16,17,20–22]. The dominant noise processes are typically Raman scattering and fluorescence caused by the pump laser and, in situations where the pump wavelength is shorter than the target wavelength, parasitic spontaneous parametric down-conversion (SPDC) driven by errors in the periodic poling [23–25]. The efficient up-conversion of this parasitic SPDC also limits the performance of converters where the target wavelength is shorter than the pump wavelength, but where the pump wavelength is located in between the two wavelengths that are converted [17]. This applies to most conversion scenarios that interconnect visible and telecommunication wavelengths. Further examples of potential building blocks of quantum networks that would benefit from a visible-wavelength-to-telecommunication-wavelength interconnect that are affected by parasitic SPDC include other color centers in diamond such as Ge-*V* (602 nm), Sn-*V* (620 nm), and Pb-*V* (520 and 555 nm) centers [7], quantum memory at 606 nm [26] and 580 nm [27], trapped ions (369.5 nm) [28], and also hexagonal boron nitride (500–850 nm, mainly around 600 nm) [29,30]. One approach to decrease the noise caused by SPDC is a two-step conversion proposed by Albota and Wong [17] and demonstrated by Esfandyarpour *et al.* [31]. A drawback of this approach is the increased complexity of the optical system, hindering the application readiness for larger-scale networks.

In our previous work, it was hypothesized that bulk periodically poled potassium titanyl phosphate (PPKTP) could prove to be a promising platform for quantum frequency conversion, owing to the comparatively high quality of the periodic poling in bulk KTP [32–34] that may help suppress parasitic SPDC processes [35]. However, waveguide converters based on PPKTP also suffer from significant parasitic SPDC noise [36], which can potentially be attributed to inhomogeneities in the waveguide geometry and a Cherenkov-idler configuration [24,37] yielding non-negligible phase matching for parasitic SPDC processes.

Here we demonstrate the potential of bulk PPKTP for efficient low-noise quantum frequency conversion from 637 nm to telecommunication wavelengths. However, the results can be applied to all conversion scenarios where the pump wavelength lies between the wavelengths that are converted. To obtain the necessary pump power for efficient conversion in a bulk crystal, the pump power was enhanced via a cavity. In particular, we used a monolithic cavity design to circumvent the requirement for active stabilization [38,39]. This passively stable, resonant enhancement of the pump enabled the use of a low-cost off-the-shelf 1064-nm continuous-wave pump laser with a power of 3 W, without introducing additional experimental complexity.

II. EXPERIMENTAL SETUP

The monolithic-bulk-PPKTP cavity was made from a 20-mm-long KTP crystal (Raicol Crystals Ltd.) quasi-phase-matched for the type-0 DFG (SFG) process 637 nm → 1064 nm + 1587 nm (or vice versa) with a domain length l of 7.85 μm. The conversion bandwidth is 110 GHz (FWHM), corresponding to 0.9 nm (0.15 nm) at 1587 nm (637 nm).

To obtain a stable pump-enhancement cavity, both end facets were polished spherically convex with a radius of curvature \mathcal{R} of 14 mm and coated to be antireflective for the red and telecommunication beams and highly reflective ($R_p = 98\%$) for the 1064-nm pump. \mathcal{R} defines the pump cavity mode to have a focusing parameter ζ_p of approximately 1.55, which, after matching of the focusing parameters for the red and telecommunication modes, leads to a Gaussian-beam reduction factor h_m of approximately 0.9 [18,19]. We measured the finesse of the cavity \mathcal{F} to be 146, which is in agreement with the predicted finesse within the fabrication tolerances. The power enhancement \mathcal{E} of 50 resulted in a maximum circulating power of about 75 W for pumping with 3 W at 1064 nm. This 75 W corresponds to an efficiency of coupling into the fundamental mode of 65%, inferred by power measurements behind the cavity. With an appropriate housing, the temperature was stabilized to below 1 mK at room temperature. The full experimental details of the conversion setup are provided in Fig. 1.

The noise floor of the converter was measured with a commercial superconducting-nanowire-single-photon-detector system (Quantum Opus LLC). Each channel had a quantum efficiency η_{det} of approximately 90% and a dark count rate of approximately 100 Hz.

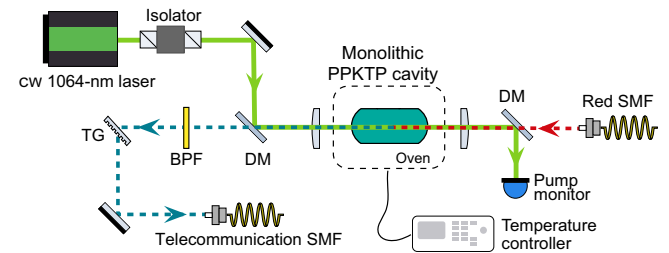


FIG. 1. Frequency-conversion setup with the monolithic-bulk-PPKTP cavity. A continuous-wave (cw) 1064-nm pump laser with power of 3 W was coupled into the monolithic PPKTP cavity. For conversion from 637 nm to the telecommunication band, the red light was launched from a SMF backwards into the PPKTP crystal, where it underwent difference-frequency generation with the back-traveling pump wave, generating light at the target telecommunication wavelength. The resulting telecommunication light was spectrally filtered via a long-pass dichroic mirror (DM), a bandpass filter (BPF; FWHM 50 nm), and a holographic transmission grating (TG). The transmitted light was then coupled into a SMF and subsequently detected.

III. RESULTS

Figure 2 shows the measured internal conversion efficiency and the generated noise spectral density (NSD) as a function of the circulating pump power. The collection bandwidth of the converter was determined by the monochromator formed by the holographic transmission grating and the aperture of the single-mode fiber (SMF), with an experimentally measured FWHM bandwidth of 0.87 nm at 1587 nm. At the maximum circulating pump power of (74.5 ± 0.3) W, the internal (external) conversion efficiency was 72% (33%) with the generation of noise of (110 ± 4) kHz/nm [(45 ± 2) kHz/nm]. This is a five-fold reduction in NSD over that of the best state-of-the-art single-step converter [16].

The measured noise counts were verified with both superconducting-nanowire single-photon detectors. We currently attribute the remaining noise in our converter to be largely due to parasitic SPDC. This is due to the noise spectrum exhibiting characteristic spectral features that can be tuned by the crystal temperature, pump polarization, and pump wavelength. Detailed investigations on this will be presented soon.

The internal conversion efficiency was determined via a power-depletion measurement of a weak red probe, and the external conversion efficiency was determined by our directly measuring the ratio between the mean photon

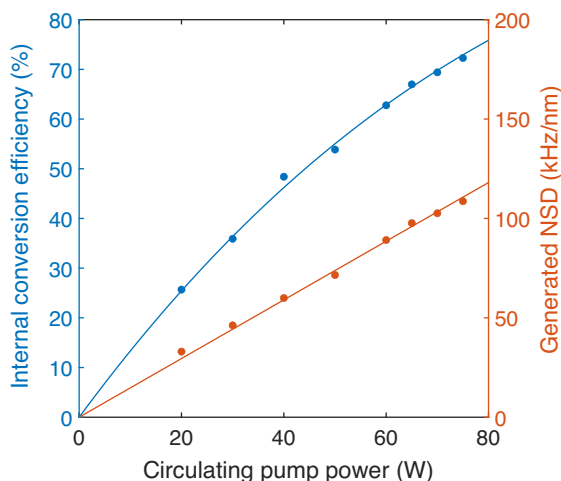


FIG. 2. Measured internal conversion efficiency (blue dots) and the generated NSD (orange dots) versus circulating pump power. The internal conversion efficiency was determined by our measuring the depletion of a weak (approximately-100- μ W) 637-nm probe laser. At the maximum circulating pump power of (74.5 ± 0.3) W, the conversion efficiency reached $(72.3 \pm 0.4)\%$. The conversion efficiency was fitted with $\sin^2(\pi/2\sqrt{P_p/P_{\max}})$, with the fit predicting 100% internal efficiency at $P_{\max} = 177$ W. The noise data were linearly fitted with a slope of 1.48 kHz/W, corresponding to a generated NSD of (110 ± 4) kHz/nm at our maximum internal efficiency of 72%.

number of an injected weak red probe and that of the converted telecommunication light coupled into a SMF. The measured internal conversion efficiency in Fig. 2 suggests $P_{\max} = 177$ W, while Eq. (1) predicts a considerably lower value, assuming a typical value for d_{eff} . We attribute this discrepancy to imperfect mode matching and alignment, and possibly spatial deformation of the modes through conversion. Accurate estimation of the generated noise spectral density, NSD_{gen} required careful accounting for the efficiencies in the experiment. The data presented in Fig. 2 were calculated with

$$\text{NSD}_{\text{gen}} = \frac{N_{\text{meas}}}{\delta\lambda\eta_{\text{col}}\eta_{\text{det}}}, \quad (2)$$

where $\eta_{\text{col}} = 33\%/72\% \approx 46\%$ was our single-mode-fiber collection efficiency of converted light or generated noise in the crystal. It resulted from the fiber coupling efficiency (72%) and the transmission through optics (99%) and filters (bandpass filter 92%, holographic transmission grating 70%). Note that a reduction in these losses by only one half with use of optimized optical components would result in a total system efficiency greater than 50%, while their further optimization together with a doubling in circulating pump power would make a total conversion efficiency of more than 80% achievable.

Because of a thermal self-tuning effect, no active stabilization was required to keep the pump on resonance and the conversion stable over hours [38,39]. The stability of the circulating pump power and of the converted signal over 60 min can be seen in Fig. 3. The observable small degradation of the conversion efficiency was due to a slow drift of the wavelength of the red probe laser used for the depletion measurement.

The converter can be used in a bidirectional manner due to the presence of the forth-and-back-traveling pump wave in the cavity. This, in principle, allows the converter to be used simultaneously for two independent conversion tasks; for example, for the conversion of polarization qubits via spatial multiplexing [40,41].

To highlight the suitability of our converter for quantum applications, we demonstrate the preservation of nonclassical correlations by the conversion process by interfacing a photon-pair source based on SPDC (see Fig. 4). A source of single photons from N-V centers in diamond was unfortunately not available at the time to test the converter. The 35-mm-long periodically poled stoichiometric lithium tantalate laser-written depressed-cladding waveguide source [42] was pumped via a continuous-wave external-cavity diode laser at 455 nm, generating pairs at 637 and 1587 nm.

Interfacing the signal photon with the converter, we obtained a peak value of the normalized cross-correlation function $g_{s,i}^{(2)}(\tau = 0)$ of 310.45 ± 0.25 . This measurement violates a Cauchy-Schwarz inequality by more than 1200

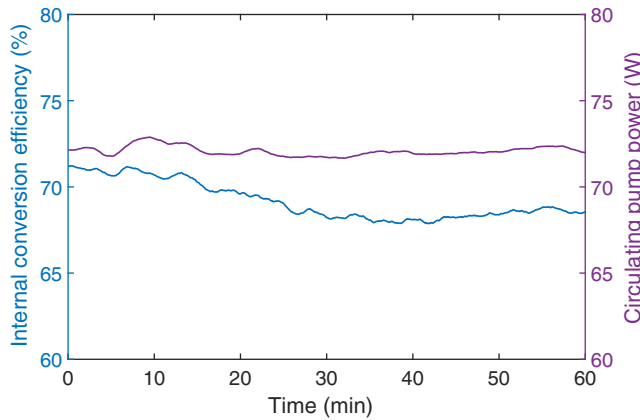


FIG. 3. Measured stability of the depleted weak probe (blue curve) and the circulating pump power (purple curve) over 60 min. The mean values of the conversion efficiency and the circulating pump power were $(69.2 \pm 1.2)\%$ and (72.1 ± 0.3) W, respectively. The small degradation of the conversion efficiency over time was due to a slow drift of the wavelength of the red probe laser.

standard deviations, indicating that the nonclassical character of the photon-pair source was preserved through conversion [36,43]. 364 kHz of singles count rate from the converter and 835 kHz singles on the other detector were measured. With a coincidence window of 1 ns, the

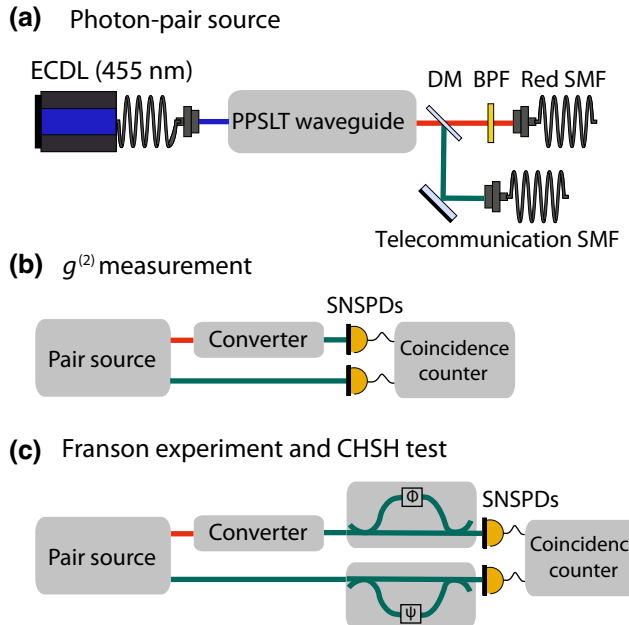


FIG. 4. (a) Photon-pair source based on a periodically poled stoichiometric lithium tantalate (PPSLT) waveguide and a blue external-cavity diode laser (ECDL). (b) Setup for the $g_{s,i}^{(2)}$ measurement including a conversion step. (c) Setup with asymmetric Mach-Zehnder interferometers before the detectors to perform a Franson experiment and the CHSH inequality test.

coincidence count rate was 18.5 kHz. See Appendix A for additional information.

To further highlight the performance of our converter, we performed a Franson experiment [44] by inserting two asymmetric Mach-Zehnder interferometers (AMZIs) into the paths of the idler and the now-down-converted signal photons. We observed raw fringe visibilities of up to $(98.2 \pm 0.1)\%$, far exceeding the classical limit of 50%. See Table I in Appendix B for the visibilities of the different port combinations.

Additionally, a more-rigorous Clauser-Horne-Shimony-Holt- (CHSH) type chained-Bell-inequality test was performed to demonstrate the preservation of time-energy entanglement by the converter. It was pointed out in Ref. [45] that standard CHSH inequalities cannot be violated in a Franson experiment due to the required postselection increasing the classical bound beyond the quantum bound. This motivated the development of chained versions of the CHSH inequality, allowing for a violation in such experiments, but requiring high fringe visibilities exceeding 94.63%. Performing a Bell test using the 10-term inequality in Ref. [45], we obtained an experimental Bell parameter S_{meas} of 9.282 ± 0.017 . Considering the local hidden variable model prediction $S_{\text{LHV}} = 9$, this violates the 10-term CHSH-type chained Bell inequality by 16σ . The quantum mechanical prediction is $S_{\text{QM}} = 9.511$. See Table II in Appendix C for the measurement results for the 6-, 8-, 10-, and 12-term inequalities.

IV. PERFORMANCE

To best illustrate the performance of our converter for a potential quantum network based on N-V centers in diamond, we show in Fig. 5 the signal-to-noise ratio (SNR) as a function of fiber transmission distance x compared with that of a noiseless converter as well as that of the current state-of-the-art PPLN-waveguide converter [16]. The simple model used for this is given by

$$\text{SNR}(x) = \frac{\eta_{\text{ext}} R_{\text{N-V}} \exp(-\alpha_t x)}{N_C \exp(-\alpha_t x) + N_D}. \quad (3)$$

Here η_{ext} includes all losses not scaling with distance: the external conversion efficiency of 33%, narrowband-filter (FWHM 5 pm) losses of 50%, and the detection efficiency of 80%. $R_{\text{N-V}}$ is the rate of single photons emitted from the N-V center in diamond, N_C is the noise rate of the converter, N_D is the dark noise rate of the detector, and α_t is the loss per distance in the telecommunication fiber. This extends the analysis of “point-to-point links,” for example, in Ref. [46], where converter noise and detector dark counts are not considered. In the example presented here, for all cases the same $R_{\text{N-V}} = 26.5$ kHz, $\eta_{\text{ext}} \approx 0.15$, $\alpha_t = -0.17$ dB/km, and $N_D = 1$ Hz were assumed. Without

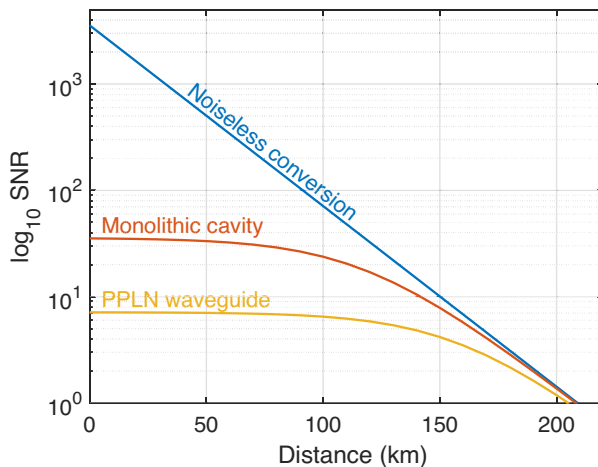


FIG. 5. Estimated SNR on a logarithmic scale as a function of fiber transmission distance for noiseless conversion (blue), the conversion noise level of the presented monolithic cavity (red), and the conversion noise level of the so-far best single-step PPLN-waveguide converter [16] (orange).

conversion of the 637-nm photons to telecommunication wavelength, the losses are so strong that the SNR would effectively drop below 1 within a few kilometers. In contrast, quantum frequency conversion not only allows for distances of up to about 150 km, but when compared with the state-of-the-art PPLN-waveguide converter [16], the bulk-PPKTP converter presented here offers a significant constant advantage that is maintained up to 100 km. Our assumed 1 Hz of detector noise starts limiting the overall SNR for the presented converter in the range of 100–150 km, diminishing the advantage of further suppressing converter noise. Above 150 km, the SNR for all three scenarios drops significantly and quantum repeater schemes become necessary [46] to maintain suitably large rates. Note that because the dark counts of the detector are assumed to be 1 Hz for noiseless conversion, the SNR is equal to the expected counts per second that can be recorded at a certain distance.

While at long distances the performance of our converter tends asymptotically towards that of an ideal converter, over shorter distances—ranges associated with metropolitan or intracity links—a considerable performance gap remains. Closing this gap requires foremost a further reduction in the noise floor of the converter, and secondarily, increases of the efficiency (both internal and external).

V. CONCLUSIONS

While bulk PPKTP has facilitated a considerable reduction in the noise floor over the existing reported values, there remains significant room for improvement for single-step converters. Detailed measurements of the noise at

the target wavelength here lead us to attribute it almost exclusively to spurious SPDC, namely, the unwanted down-conversion of the strong 1064-nm pump to a signal photon at the target wavelength and an idler in the mid-IR range. One might think shifting from quasi-phase-matching to birefringent phase matching would therefore offer a solution, but in doing so, one both loses access to the comparatively strong d_{33} tensor element and introduces double refraction, requiring much-higher (an order of magnitude more) pump powers and experimental complexity and lower scalability, all the while limiting the intrinsically attainable maximum conversion efficiency significantly below 100%. Instead, approaches that focus on direct suppression of the unwanted SPDC processes in periodically poled crystals could involve resonantly enhancing the signal field, which would dramatically lower the required circulating pump power. Alternatively or additionally, one could realize schemes with strong absorption of, or utilizing antiresonant cavity suppression of, the parasitic mid-IR idler field.

In conclusion, we have presented an efficient low-noise quantum frequency converter based on a monolithic-bulk-PPKTP cavity suitable for the conversion of single photons from nitrogen-vacancy centers in diamond to telecommunication wavelength. Together with the compact and self-stabilizing design and requiring only cost-effective and off-the-shelf commercial pump lasers, our QFC platform represents a viable technological ingredient for improved scalability of future quantum networks. During the review process for this publication, the authors became aware of a relevant preprint on low-noise conversion using an unpoled potassium titanyl arsenate crystal [47].

ACKNOWLEDGMENTS

We thank Martin Jutisz, Max Tillmann, Florian Kaiser, and Janik Wolters for helpful discussions and technical support. This work was funded by the BMBF, Germany, within the project QR.X.

The authors declare no conflicts of interest.

APPENDIX A: $g_{s,i}^{(2)}$ MEASUREMENT

Figure 6 shows the measured un-normalized cross-correlation function after the down-conversion of the signal photon. From this, a peak value of the normalized cross-correlation function $g_{s,i}^{(2)}(\tau = 0) = 310.45 \pm 0.25$ was obtained. The small side lobes evident in Fig. 6 at ± 500 ps from the center peak are attributed to residual reflections in the detection electronics.

APPENDIX B: THE FRANSON EXPERIMENT

Figure 7 shows the measured raw coincidences in the Franson experiment. In Table I all visibilities of the differ-

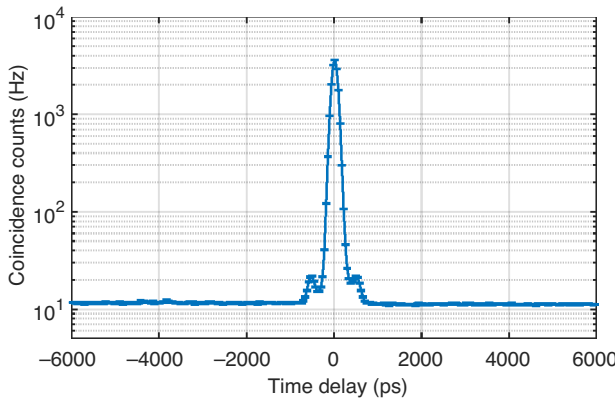


FIG. 6. Measured un-normalized cross-correlation function $G_{s,i}^{(2)}$ of the photon pairs after the conversion with error bars for the standard errors.

ent output-port combinations from the Franson experiment are listed. Raw (corrected) visibilities are without (with) the subtraction of the background formed by accidental coincidences.

APPENDIX C: THE CHAINED BELL INEQUALITIES

A CHSH-type chained-Bell-inequality test was performed to demonstrate the preservation of time-energy entanglement by the converter. It was pointed out that standard CHSH inequalities cannot be violated in a Franson experiment due to the required postselection increasing the classical bound beyond the quantum bound [45,48]. This postselection loophole would even allow for faking of the

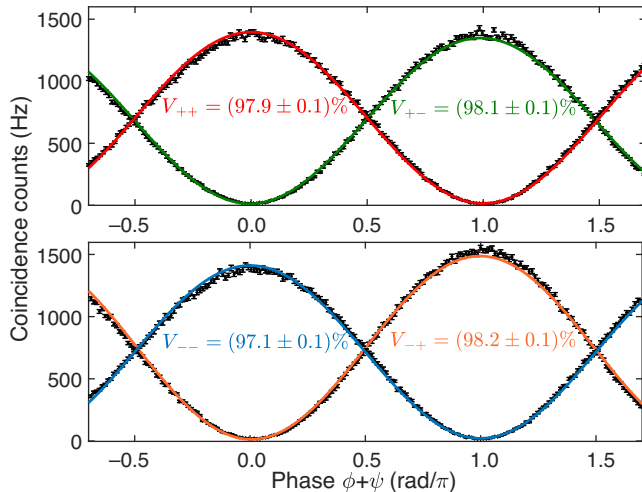


FIG. 7. Measured raw coincidences in the Franson experiment with postselection over detuned phase $\psi + \phi$ for all four port combinations with error bars for the standard errors. $\cos^2(x)$ functions were fitted to extract the visibility. A raw fringe visibility of the fits of about 98% was achieved (see Table I).

TABLE I. Visibilities in the Franson experiment.

Port	Raw visibility (%)	Corrected visibility (%)
++	97.9 ± 0.1	98.5 ± 0.1
+-	98.1 ± 0.1	98.7 ± 0.1
--	97.1 ± 0.1	97.7 ± 0.1
-+	98.2 ± 0.1	98.8 ± 0.2

violation of the CHSH inequality with classical light [49] and thus cannot serve as an entanglement witness [50,51] without additional assumptions being made.

Nonetheless, chained versions of the CHSH inequality were developed [52–54], allowing for a violation in experiments, but requiring very high fringe visibilities exceeding 94.63%. A postselection-loophole-free Bell violation with genuine time-bin entanglement was performed recently [53]. The chained CHSH inequality for N measurement settings and $2N$ terms is given by [54]

$$S^N \leq S_{\text{LHV}}^N, \quad (\text{C1})$$

$$S^N = \langle A_N B_N \rangle + \sum_{k=2}^N [\langle A_k B_{k-1} \rangle + \langle A_{k-1} B_k \rangle] - \langle A_1 B_1 \rangle. \quad (\text{C2})$$

The upper bound for local hidden-variable theories is $S_{\text{LHV}}^N = 2N - 1$, while quantum theory predicts $S_{\text{QM}}^N = 2N \cos(\pi/2N)$. The strongest violation by quantum mechanics is given for a relative angle $\theta = \phi + \psi = \pi/2N$. The critical visibility that has to be surpassed experimentally is given by $V_{\text{crit}} = S_{\text{LHV}}^N / S_{\text{QM}}^N$. See Table II for all results.

In our experiment, we did not have a closed-loop phase control with stabilization light [54]. Keeping a phase setting stable was working well but the repeatability of setting a phase was not ideal. This is due to the properties of an open-loop piezoelectric positioning-system. Since each phase-measurement operator A_j and B_j appears twice in the chained Bell inequality, each phase setting can just be kept to record two expectation values. This may lead to unideal relative angles θ and thus decrease the violation but it is allowed by Eqs. (C1) and (C2). Not choosing the phase settings pairwise (but choosing them

TABLE II. Chained-Bell-inequality violations.

N	S_{LHV}^N	S_{QM}^N	$V_{\text{crit}} (\%)$	S_{meas}^N	Violation
2	3	2.828	> 100	2.755 ± 0.020	...
3	5	5.196	96.23	5.039 ± 0.017	2σ
4	7	7.391	94.71	7.270 ± 0.017	15σ
5	9	9.511	94.63	9.282 ± 0.017	16σ
6	11	11.59	94.90	11.335 ± 0.018	18σ

independently) as dictated by these equations, on the other hand, would increase S_{LHV} . Only the last term has one phase setting of the first term and thus requires repeatability. In our measurements, we took care of the lack of repeatability by recording each chained Bell inequality 10 times and averaging over these trials. Further, the expectation values in the experiment are given by $E = (R_{++} - R_{+-} - R_{-+} + R_{--})/(R_{++} + R_{+-} + R_{-+} + R_{--})$, where R are the rates again and the first index corresponds to AMZI 1 and the second index corresponds to AMZI 2 with ports “+” and “-” each. We had only two instead of four detectors available to monitor the four output ports of the interferometers. Thus, we assumed $R_{++} = R_{--}$, $R_{+-} = R_{-+}$ and $R_{+-} = R_{++}^\pi$ [54]. Also, no fast random switching of the phases on the timescale of 1.25 GHz was used here. The greatest frequency that would in principle be allowed by the piezoelectric actuators is 50 kHz.

-
- [1] P. Kumar, Quantum frequency conversion, *Opt. Lett.* **15**, 1476 (1990).
 - [2] H. J. Kimble, The quantum internet, *Nature* **453**, 1023 (2008).
 - [3] D. Awschalom, K. K. Berggren, H. Bernien, S. Bhade, L. D. Carr, P. Davids, S. E. Economou, D. Englund, A. Faraon, M. Fejer, *et al.*, Development of quantum interconnects (QuICs) for next-generation information technologies, *PRX Quantum* **2**, 017002 (2021).
 - [4] L.-M. Duan and C. Monroe, Colloquium: Quantum networks with trapped ions, *Rev. Mod. Phys.* **82**, 1209 (2010).
 - [5] A. Reiserer and G. Rempe, Cavity-based quantum networks with single atoms and optical photons, *Rev. Mod. Phys.* **87**, 1379 (2015).
 - [6] P. Lodahl, Quantum-dot based photonic quantum networks, *Quantum Sci. Technol.* **3**, 013001 (2017).
 - [7] M. Ruf, N. H. Wan, H. Choi, D. Englund, and R. Hanson, Quantum networks based on color centers in diamond, *J. Appl. Phys.* **130**, 070901 (2021).
 - [8] L. Childress and R. Hanson, Diamond NV centers for quantum computing and quantum networks, *MRS Bull.* **38**, 134 (2013).
 - [9] K. Nemoto, M. Trupke, S. J. Devitt, B. Scharfenberger, K. Buczak, J. Schmiedmayer, and W. J. Munro, Photonic quantum networks formed from NV-centers, *Sci. Rep.* **6**, 26284 (2016).
 - [10] G. Balasubramanian, P. Neumann, D. Twitchen, M. Markham, R. Kolesov, N. Mizuochi, J. Isoya, J. Achard, J. Beck, and J. Tissler, *et al.*, Ultralong spin coherence time in isotopically engineered diamond, *Nat. Mater.* **8**, 383 (2009).
 - [11] M. G. Dutt, L. Childress, L. Jiang, E. Togan, J. Maze, F. Jelezko, A. Zibrov, P. Hemmer, and M. Lukin, Quantum register based on individual electronic and nuclear spin qubits in diamond, *Science* **316**, 1312 (2007).
 - [12] P. C. Maurer, G. Kucsko, C. Latta, L. Jiang, N. Y. Yao, S. D. Bennett, F. Pastawski, D. Hunger, N. Chisholm, M. Markham, *et al.*, Room-temperature quantum bit memory exceeding one second, *Science* **336**, 1283 (2012).
 - [13] C. Bradley, S. de Bone, P. Möller, S. Baier, M. Degen, S. Loenen, H. Bartling, M. Markham, D. Twitchen, and R. Hanson, *et al.*, Robust quantum-network memory based on spin qubits in isotopically engineered diamond, *npj Quantum Inf.* **8**, 122 (2022).
 - [14] M. W. Doherty, N. B. Manson, P. Delaney, F. Jelezko, J. Wrachtrup, and L. C. Hollenberg, The nitrogen-vacancy colour centre in diamond, *Phys. Rep.* **528**, 1 (2013).
 - [15] M. Pompili, S. L. Hermans, S. Baier, H. K. Beukers, P. C. Humphreys, R. N. Schouten, R. F. Vermeulen, M. J. Tiggelman, L. dos Santos Martins, B. Dirkse, *et al.*, Realization of a multimode quantum network of remote solid-state qubits, *Science* **372**, 259 (2021).
 - [16] A. Dréau, A. Tchekbotareva, A. El Mahdaoui, C. Bonato, and R. Hanson, Quantum frequency conversion of single photons from a nitrogen-vacancy center in diamond to telecommunication wavelengths, *Phys. Rev. Appl.* **9**, 064031 (2018).
 - [17] M. A. Albota and F. N. Wong, Efficient single-photon counting at 1.55 μm by means of frequency upconversion, *Opt. Lett.* **29**, 1449 (2004).
 - [18] G. Boyd and D. Kleinman, Parametric interaction of focused Gaussian light beams, *J. Appl. Phys.* **39**, 3597 (1968).
 - [19] S. Guha and J. Falk, The effects of focusing in the three-frequency parametric upconverter, *J. Appl. Phys.* **51**, 50 (1980).
 - [20] R. Ikuta, T. Kobayashi, S. Yasui, S. Miki, T. Yamashita, H. Terai, M. Fujiwara, T. Yamamoto, M. Koashi, M. Sasaki, *et al.*, Frequency down-conversion of 637 nm light to the telecommunication band for non-classical light emitted from NV centers in diamond, *Opt. Express* **22**, 11205 (2014).
 - [21] P. C. Strassmann, A. Martin, N. Gisin, and M. Afzelius, Spectral noise in frequency conversion from the visible to the telecommunication C-band, *Opt. Express* **27**, 14298 (2019).
 - [22] N. Maring, D. Lago-Rivera, A. Lenhard, G. Heinze, and H. de Riedmatten, Quantum frequency conversion of memory-compatible single photons from 606 nm to the telecom C-band, *Optica* **5**, 507 (2018).
 - [23] J. S. Pelc, C. Phillips, D. Chang, C. Langrock, and M. Fejer, Efficiency pedestal in quasi-phase-matching devices with random duty-cycle errors, *Opt. Lett.* **36**, 864 (2011).
 - [24] J. S. Pelc, C. Langrock, Q. Zhang, and M. Fejer, Influence of domain disorder on parametric noise in quasi-phase-matched quantum frequency converters, *Opt. Lett.* **35**, 2804 (2010).
 - [25] M. M. Fejer, G. Magel, D. H. Jundt, and R. L. Byer, Quasi-phase-matched second harmonic generation: Tuning and tolerances, *IEEE J. Quantum Electron.* **28**, 2631 (1992).
 - [26] K. Kutluer, M. Mazzera, and H. de Riedmatten, Solid-state source of nonclassical photon pairs with embedded multimode quantum memory, *Phys. Rev. Lett.* **118**, 210502 (2017).
 - [27] C. Laplane, P. Jobez, J. Etesse, N. Gisin, and M. Afzelius, Multimode and long-lived quantum correlations between photons and spins in a crystal, *Phys. Rev. Lett.* **118**, 210501 (2017).

- [28] D. L. Moehring, P. Maunz, S. Olmschenk, K. C. Younge, D. N. Matsukevich, L.-M. Duan, and C. Monroe, Entanglement of single-atom quantum bits at a distance, *Nature* **449**, 68 (2007).
- [29] T. T. Tran, K. Bray, M. J. Ford, M. Toth, and I. Aharonovich, Quantum emission from hexagonal boron nitride monolayers, *Nat. Nanotechnol.* **11**, 37 (2016).
- [30] J. D. Caldwell, I. Aharonovich, G. Cassabois, J. H. Edgar, B. Gil, and D. Basov, Photonics with hexagonal boron nitride, *Nat. Rev. Mater.* **4**, 552 (2019).
- [31] V. Esfandyarpour, C. Langrock, and M. Fejer, Cascaded downconversion interface to convert single-photon-level signals at 650 nm to the telecom band, *Opt. Lett.* **43**, 5655 (2018).
- [32] C. Canalias, J. Hirohashi, V. Pasiskevicius, and F. Laurill, Polarization-switching characteristics of flux-grown KTiOPO_4 and RbTiOPO_4 at room temperature, *J. Appl. Phys.* **97**, 124105 (2005).
- [33] P. Mutter, A. Zukauskas, and C. Canalias, Domain dynamics in coercive-field engineered sub- μm periodically poled Rb-doped kTiOPO_4 , *Opt. Mater. Express* **12**, 4332 (2022).
- [34] P. Mutter, K. M. Mølster, A. Zukauskas, V. Pasiskevicius, and C. Canalias, Highly-efficient first-order backward second-harmonic generation in periodically poled Rb-doped KTP with a period of 317 nm, *Nonlinear Photonics* (2022). NpTu1G.
- [35] F. Mann, H. M. Chrzanowski, and S. Ramelow, Low random duty-cycle errors in periodically poled KTP revealed by sum-frequency generation, *Opt. Lett.* **46**, 3049 (2021).
- [36] H. Rütz, K.-H. Luo, H. Suche, and C. Silberhorn, Quantum frequency conversion between infrared and ultraviolet, *Phys. Rev. Appl.* **7**, 024021 (2017).
- [37] V. Rastogi, K. Thyagarajan, M. Shenoy, P. Baldi, M. De Micheli, and D. Ostrowsky, Modeling of large-bandwidth parametric amplification in the Čerenkov-idler configuration in planar waveguides, *JOSA B* **14**, 3191 (1997).
- [38] J. A. Zielińska and M. W. Mitchell, Self-tuning optical resonator, *Opt. Lett.* **42**, 5298 (2017).
- [39] J. A. Zielińska, A. Zukauskas, C. Canalias, M. A. Noyan, and M. W. Mitchell, Fully-resonant, tunable, monolithic frequency conversion as a coherent UVA source, *Opt. Express* **25**, 1142 (2017).
- [40] S. Ramelow, A. Fedrizzi, A. Poppe, N. K. Langford, and A. Zeilinger, Polarization-entanglement-conserving frequency conversion of photons, *Phys. Rev. A* **85**, 013845 (2012).
- [41] M. Bock, S. Kucera, P. Eich, M. Kreis, A. Lenhard, J. Eschner, and C. Becher, Polarization-preserving quantum frequency conversion for entanglement distribution in trapped-atom based quantum networks, *Quantum Inf. Meas.* (2019). T5A.
- [42] L. Li, W. Kong, and F. Chen, Femtosecond laser-inscribed optical waveguides in dielectric crystals: A concise review and recent advances, *Adv. Photonics* **4**, 024002 (2022).
- [43] M. Reid and D. Walls, Violations of classical inequalities in quantum optics, *Phys. Rev. A* **34**, 1260 (1986).
- [44] J. D. Franson, Bell inequality for position and time, *Phys. Rev. Lett.* **62**, 2205 (1989).
- [45] J. Jogenfors and J.-Å. Larsson, Energy-time entanglement, elements of reality, and local realism, *J. Phys. A: Math. Theor.* **47**, 424032 (2014).
- [46] P. van Loock, W. Alt, C. Becher, O. Benson, H. Boche, C. Deppe, J. Eschner, S. Höfling, D. Meschede, P. Michler, *et al.*, Extending quantum links: Modules for fiber-and memory-based quantum repeaters, *Adv. Quantum Technol.* **3**, 1900141 (2020).
- [47] J. Geus, F. Elsen, S. Nyga, A. Stolk, K. van der Enden, E. van Zwet, C. Haefner, R. Hanson, and B. Jungbluth, Low-noise short-wavelength pumped frequency down-conversion for quantum frequency converters, *Opt. Open* 107563 (2023).
- [48] S. Aerts, P. Kwiat, J.-Å. Larsson, and M. Zukowski, Two-photon Franson-type experiments and local realism, *Phys. Rev. Lett.* **83**, 2872 (1999).
- [49] J. Jogenfors, A. M. Elhassan, J. Ahrens, M. Bourennane, and J.-Å. Larsson, Hacking the Bell test using classical light in energy-time entanglement-based quantum key distribution, *Sci. Adv.* **1**, e1500793 (2015).
- [50] P. Hyllus, O. Gühne, D. Bruß, and M. Lewenstein, Relations between entanglement witnesses and Bell inequalities, *Phys. Rev. A* **72**, 012321 (2005).
- [51] B. M. Terhal, Bell inequalities and the separability criterion, *Phys. Lett. A* **271**, 319 (2000).
- [52] S. L. Braunstein and C. M. Caves, Wrapping out better Bell inequalities, *Ann. Phys.* **202**, 22 (1990).
- [53] F. Vedovato, C. Agnesi, M. Tomasin, M. Avesani, J.-Å. Larsson, G. Vallone, and P. Villoresi, Postselection-loophole-free Bell violation with genuine time-bin entanglement, *Phys. Rev. Lett.* **121**, 190401 (2018).
- [54] M. Tomasin, E. Mantoan, J. Jogenfors, G. Vallone, J.-Å. Larsson, and P. Villoresi, High-visibility time-bin entanglement for testing chained Bell inequalities, *Phys. Rev. A* **95**, 032107 (2017).